The good? The bad? The mutant! Characterization of cancer-related somatic mutations and identification of a selectivity hotspot in adenosine receptor

Wang, X.

Chapter 5

Cancer-related somatic mutations alter adenosine A_1 receptor pharmacology.
- a focus on mutations in the loops and C-terminus.

This chapter is based upon:
Xuesong Wang, Willem Jespers, Just J. de Waal, Kim A.N. Wolff, Liedeke van Uden, Adriaan P. IJzerman, Gerard J.P. van Westen and Laura H. Heitman
The FASEB Journal. **2022**, 36:e22358

Abstract

G protein-coupled receptors (GPCRs) are known to be involved in tumor progression and metastasis. The adenosine A_1 receptor (A_1AR) has been detected to be over-expressed in various cancer cell lines. However, the role of A_1AR in tumor development is not yet well characterized. A series of A_1AR mutations were identified in the Cancer Genome Atlas from cancer patient samples. In this study, we have investigated the pharmacology of mutations located outside of the 7-transmembrane domain by using a 'single-GPCR-one-G protein' yeast system. Concentration-growth curves were obtained with the full agonist CPA for 12 mutant receptors and compared to the wild-type hA_1AR. Most mutations located at the extracellular loops (EL) reduced the levels of constitutive activity of the receptor and agonist potency. For mutants at the intracellular loops (IL) of the receptor, an increased constitutive activity was found for mutant receptor L211R$^{5.69}$, while a decreased constitutive activity and agonist response were found for mutant receptor L113F$^{34.51}$. Lastly, mutations identified on the C-terminus did not significantly influence the pharmacological function of the receptor. A selection of mutations was also investigated in a mammalian system. Overall, similar effects on receptor activation compared to the yeast system were found with mutations located at the EL, but some contradictory effects were observed for mutations located at the IL. Taken together, this study will enrich the insight of A_1AR receptor structure and function, enlightening the consequences of these mutations in cancer. Ultimately, this may provide potential precision medicine in cancer treatment.

Keywords: G protein-coupled receptors, adenosine A_1 receptor, cancer, mutations, yeast system

Introduction

G protein-coupled receptors (GPCRs) are the largest family of membrane-bound proteins in the human genome with approximately 800 subtypes[1]. They share a common structure of seven-transmembrane helices (TMs) linked by three extracellular loops (ELs) and three intracellular loops (ILs) together with an extracellular N-terminus and an intracellular C-terminus[2]. GPCRs regulate various cellular and physiological effects via responding to a diverse set of endogenous ligands[3]. However, their aberrant activity and expression also contribute to some of the most prevalent human diseases[4].

In preclinical oncology, kinases have been studied as primary focus due to their central roles in the cell cycle[5]. GPCRs, on the other hand, have been relatively under-investigated over the last two decades. Yet, an increasing amount of evidence shows that GPCRs are also prominently involved in all phases of cancer[6]. Additionally, the normal physiological function of GPCRs is often hijacked by malignant cells to survive as well as to invade surrounding tissue and evade the immune system[7]. Moreover, a systematic analysis of somatic mutations in cancer genomes has led to the discovery that GPCRs are mutated in an estimated 20% of all cancers[5]. Combined, these observations warrant a close investigation of the role of GPCRs in cancer.

Adenosine is a ubiquitous purine nucleoside that mediates its physiological effects via the adenosine receptors (ARs); the A_1, the A_{2A}, the A_{2B}, and the A_3 receptor. The A_1AR and A_3AR mainly recruit a G_i protein and inhibit adenylate cyclase, while the A_{2A}AR and A_{2B}AR stimulate adenylate cyclase through coupling to a G_s protein[8]. It is known that the immune system plays a fundamental and essential role in the defense against cancer, yet the mechanisms have not been fully characterized. Adenosine and ARs have been reported to be involved in the immune response in cancer[9]. Additionally, ARs are expressed diversely in various tumor types[10]. Compared to healthy tissue, adenosine concentrations are increased by more than 50 fold in the hypoxic tumor environment[11]. Therefore, all four subtypes of ARs may be activated in cancer and may play a role in cancer progression.

A_1AR has mainly been under investigation as a drug target for pathologies in brain, heart, kidney and fat cells, due to its high expression in these cells/organs[12,13]. Growing evidence suggests that the A_1AR is also involved in cancer progression, although its role is not well understood and sometimes observations are inconsistent[13,14]. An increased expression level of the A_1AR has been observed in diverse cancer cells[15–17]. In MCF7 breast cancer cells, activation of the A_1AR leads to decreased apoptosis and thereby induces tumor growth[17]. In renal cell carcinoma, cell proliferation and migration is inhibited by an A_1AR antagonist through the ERK/JNK signaling pathway[15]. Conversely, the stimulation of A_1AR significantly decreases tumor cell proliferation in CW2 colonic cell tumor and glioblastomas[18,19]. An RNA interference study on breast cancer cells indicates that depletion of A_1AR results in more apoptosis[16]. Taken together, it appears that A_1AR activation induces both

anti- and pro-tumoral effects in cancer development[11]. Various mutations have been identified on A_1AR from patient samples with different cancer types[20]. Mutations in A_1AR are known to alter the receptor-ligand interaction, receptor constitutive activity and agonist-mediated receptor activation[21]. Notably, these function-altering mutations can be located all over the protein, including the TMs, ELs and ILs[22]. Based on the altered constitutive activity independent of an agonist, mutant receptors with increased level of activation are referred to as constitutively active mutants (CAMs), while those with lowered level are named constitutively inactive mutants (CIMs)[23].

In the present study, 12 mutations, which were located in ELs, ILs, and C-terminus of the A_1AR, were selected from cancer patients using a bioinformatics approach. These mutant receptors were tested in an *S. cerevisiae* strain to study the effect of them on receptor activation. Subsequently, some mutant receptors were further investigated for their effect on ligand binding and receptor activation in a mammalian system. Based on the pharmacological effects of these mutant receptors, we identified 1 CAM and 7 CIMs. In addition, we found 1 loss-of-function mutant (LFM) and 3 mutant receptors, which were functionally indistinguishable from the wild-type hA_1AR (no effect mutants, NEMs).

Materials and methods

Data mining

Data was downloaded from The Cancer Genome Atlas (TCGA, version August 8th 2015) via the Firehose tool[24]. MutSig 2.0 data was extracted, but MutSig 2CV was used when the former was not available (the case for colon adenocarcinoma, acute myeloid leukemia, ovarian serous cystadenocarcinoma, rectum adenocarcinoma). In parallel natural variance data was downloaded from Uniprot (Index of Protein Altering Variants, version November 11th 2015)[25]. Somatic mutations were selected from the sequence data and filters were applied to only select data for the A_1AR (Uniprot identifier P30542). The GPCRdb alignment tool was used to assign Ballesteros-Weinstein numbers[26,27] to the positions through which a selection could be made for non-TM domain positions.

Materials

The MMY24 strain and the *S. cerevisiae* expression vectors, the pDT-PGK plasmid and the pDT-PGK_hA_1AR plasmid (i.e. expressing by coding for the wild-type hA_1AR) were kindly provided by Dr. Simon Dowell from GSK (Stevenage, UK). The QuikChange II® Site-Directed Mutagenesis Kit was purchased from Agilent Technologies, which includes XL10-Gold ultracompetent cells (Amstelveen, the Netherlands). The QIAprep mini plasmid purification kit and QIAGEN® plasmid midi kit were purchased from QIAGEN (Amsterdam, the Netherlands). Adenosine deaminase (ADA), 1,4-dithiothreitol (DTT), 8-cyclopentyl-1,3-dipropylxanthine

(DPCPX) and 3-amino-[1,2,4]-triazole (3-AT) were purchased from Sigma-Aldrich (Zwijndrecht, the Netherlands). N^6-cyclopentyladenosine (CPA) was purchased from Santa Cruz Biotechnology (Heidelberg, Germany). Radioligand 1,3-[^{3}H]-dipropyl-8-cyclopentylxanthine ([^{3}H]DPCPX, specific activity of 120 Ci × mmol^{-1}) was purchased from ARC Inc. (St. Louis, MO). Bicinchoninic acid (BCA) and BCA protein assay reagent were obtained from Pierce Chemical Company (Rockford, IL, USA). [^{35}S]-Guanosine 5'-(γ-thio)triphosphate ([^{35}S]GTPγS, specific activity 1250 Ci × mmol^{-1}) was purchased from PerkinElmer, Inc. (Waltham, MA, USA). Rabbit anti-HA antibody (71-5500) was purchased from Thermo Fisher Scientific (Waltham, MA, USA). Goat anti-rabbit IgG Fc (Alexa Fluor® 647) was purchased from Abcam (Cambridge, UK).

Generation of hA$_1$AR mutations

Mutant hA$_1$ARs were generated by polymerase chain reaction (PCR) mutagenesis as previously described[28]. pDT-PGK_hA$_1$AR or pcDNA3.1(+)_hA$_1$AR with N-terminal HA tag was used as the template[21,29]. Primers for mutant receptors were designed by the QuikChange Primer Design Program of Agilent Technologies (Santa Clara, CA, USA) and primers were obtained from Eurogentec (Maastricht, The Netherlands). All DNA sequences were verified by Sanger sequencing at LGTC (Leiden, The Netherlands).

Transformation in MMY24 S. cerevisiae strain

The plasmids, pDT-PGK_hA$_1$AR, containing either wild-type or mutant hA$_1$AR were transformed into a MMY24 *S. cerevisiae* strain using the Lithium-Acetate procedure[30].

Liquid growth assay

To characterize the mutant hA$_1$ARs, concentration-growth curves were obtained from a liquid growth assay in 96-well plates as previously described[21]. Briefly, selective medium lacking uracil and leucine (YNB-UL, 1ml) was inoculated with yeast cells expressing wild-type or mutant hA$_1$AR. After overnight incubation at 30 °C, the cultures were diluted to 40,000 cells/ml (OD_{600} ≈ 0.02) in selective medium without histidine (YNB-ULH).Various concentrations of ligands (2 *μL*), yeast cells (50 *μL*) and YNB-ULH medium containing 7 mM 3-AT and 0.8 IU/ml ADA (150 *μL*) were added to each well. Then, the 96-well plate was incubated at 30 °C for 35 h in a Genios plate reader while shaking for 1 min at 300 rpm every 10 min.

Cell culture, transient transfection and membrane preparation

Chinese hamster ovary (CHO) cells were cultured in Dulbecco's modified Eagle's medium/Ham's F12 (1:1, DMEM/F12) containing 10% bovine calf serum, streptomycin (50 μg/mL) and penicillin (50 IU/mL) at 37 °C in 5% CO_2. The cells were subcultured twice weekly at a ratio of 1:30. 24 h before transfection, cells were seeded in 10-cm culture dishes containing 10 mL culture medium to achieve 50-60% confluency. Cells were then transfected with plasmid DNA (10 μg/dish) by the PEI method with a PEI:DNA ratio of 3:1[31]. 24 h after transfection, the medium was refreshed by 10

mL fresh culture medium. After an additional 24 h incubation at 37 °C in 5% CO_2, cells were collected and membranes were prepared as described previously[32]. Membranes were then aliquoted in 250 or 100 µL and stored at -80 °C till further use. Membrane protein concentrations were measured by the BCA method[33].

Western blot analysis

Membranes containing 8.5 µg protein were denatured in 1x Laemmli sample buffer before loading. Samples were separated on a 12.5% SDS/PAGE gel and then electro-blotted onto polyvinylidene fluoride (PVDF) membranes via Bio-Rad Trans-blot® Turbo™ transfer system. After blocking with 5% BSA in TBST (0.05% Tween 20 in Tris-buffered saline), the membranes were incubated with rabbit anti-HA tag primary antibody (1:2000, Thermo Fisher Scientific) in TBST containing 1% BSA at 4 °C for overnight. The membranes were then washed three times in TBST and incubated with goat anti-rabbit IgG Fc (1:7500, Alexa Fluor® 647) in TBST containing 1% BSA for 1 hour at room temperature, followed by washing twice in TBST and once in TBS. Images of the blots were taken with a ChemiDoc MP imaging system (Hercules, CA, USA) using a Cy5 filter.

Radioligand displacement assay

The displacement assays were performed as described previously[34]. Briefly, experiments were performed in a total volume of 100 µL, consisting of 25 µL cell membranes (10 – 25 µg protein to achieve an assay window of approximately 1500 DPM), 25 µL of radioligand [^{3}H]DPCPX with a final concentration of ~1.6 nM, 25 µL of assay buffer (50 mM Tris-HCl, pH 7.4) and 25 µL of DPCPX or CPA in 6 or 10 increasing concentrations (final concentrations of 10^{-11} to 10^{-6} M and 10^{-10} to 10^{-5} M, respectively) in assay buffer, and incubated for 1h at 25 °C. Nonspecific binding was determined in the presence of 100 µM CPA and represented less than 10% of the total binding. For homologous competition assays, radioligand displacement experiments were done in the presence of three concentrations of [^{3}H]DPCPX (final concentrations of ~1.6 nM, 4.5 nM and 10 nM) and 6 increasing concentrations of DPCPX (final concentration of 10^{-11} to 10^{-6} M). After incubation, reactions were terminated by rapid vacuum filtration through GF/B filter plates (PerkinElmer, Groningen, Netherlands) using a Perkin Elmer Filtermate-harvester. Filter plates were subsequently washed ten times with ice-cold buffer (50 mM Tris-HCl, pH 7.4). After drying the filter plates at 55 °C for 30 min, the filter-bound radioactivity was determined by scintillation spectrometry using a Microbeta2® 2450 microplate counter (PerkinElmer).

[^{35}S]GTPγS binding assay

[^{35}S]GTPγS binding assays were adapted from a previously reported method[34]. Experiments were performed in a total volume of 80 µL assay buffer (50 mM Tris-HCl buffer, 5 mM $MgCl_2$, 1 mM EDTA, 100 mM NaCl, 0.05% BSA and 1 mM DTT pH 7.4 supplemented with 10 **µM** GDP, 10 µg saponin), consisting of 20 µL membranes (15 µg protein), 20 µL of CPA in 9 increasing concentrations (final concentrations

of 10^{-11} to 10^{-6} M) or 20 µL of DPCPX (final concentrations of 10^{-11} to 10^{-6} M) in 9 increasing concentrations combined with a fixed concentration (EC_{80} for wild-type or mutant hA_1ARs) of CPA, and incubated for 30 min at 4 °C. Then 20 µL of [^{35}S]GTPγS (final concentration of 0.3 nM) was added and followed by 90 min incubation at 25 °C. Incubation was terminated and filter-bound activity was determined as described above.

Modelling

Figures were created based on the experimentally determined structures for the A_1AR crystal structures, with PDB codes 5UEN[35] for the inactive and 6D9H[36] for the fully active structure. DPCPX and CPA were manually docked based on high similarity with the co-crystallized ligands in the respective structures, and figures were generated using the PyMOL Molecular Graphics System version 2.0 (Schrödinger, LLC., USA).

Data analysis

All experimental data were analyzed by GraphPad Prism 7.0 software (GraphPad Software Inc., San Diego, CA, USA). Liquid growth assays and [^{35}S]GTPγS binding assay were analyzed by non-linear regression using a "log (agonist or inhibitor) vs. response (three parameters)" model to obtain potency (EC_{50}), inhibitory potency (IC_{50}) and efficacy (E_{max}) values. Homologous competition assays were analyzed by non-linear regression using a "one-site homologous" model to obtain pK_D and B_{max} values. Radioligand displacement curves were analyzed by non-linear regression using a "one site - IC50" or "two site – IC50" model to obtain pIC_{50} values. pK_i values were calculated from pIC_{50} values using the Cheng-Prusoff equation[37].

Results

Data mining

Mutation data from cancer patient isolates of a selection of cancer types, i.e. breast invasive carcinoma, colon adenocarcinoma, lung adenocarcinoma, lung squamous cell carcinoma, lymphoid neoplasm diffuse large B-cell lymphoma and rectum adenocarcinoma, were obtained by data mining the TCGA database on August 8th 2015. This resulted in a selection of 27 somatic point mutations for the hA_1AR out of a total of 48 cancer-related mutations of hA_1AR. After assigning Ballesteros Weinstein numbers to the positions by using the GPCRdb alignment tool, 12 mutations located outside the 7-TM domains were selected for this study (Table 1). Five mutations were located at the second EL, four at the IL and three at the C-terminus of hA_1AR, which are shown in the snake-plot in Figure 1A.

Table 1. List of cancer-related somatic mutations identified from different cancer types.

Mutations	Cancer types
N148S^{EL2}	Lung adenocarcinoma
A151V ^{EL2}	Lymphoid neoplasm diffuse large B-cell lymphoma
V152L ^{EL2}	Lung adenocarcinoma
E170G$^{45.51}$	Colon adenocarcinoma
M177V$^{5.37}$	Lung adenocarcinoma
L113F$^{34.51}$	Lung squamous cell carcinoma
L211R$^{5.69}$	Lung adenocarcinoma
V215L^{IL3}	Lung adenocarcinoma
D221N^{IL3}	Lung squamous cell carcinoma
H306N$^{8.61}$	Colon adenocarcinoma
R308H$^{8.63}$	Lung adenocarcinoma
I315V$^{C\text{-}term}$	Lung squamous cell carcinoma

Constitutive activity of mutant hA$_1$ARs

To characterize the effect of the cancer-related mutations on the constitutive activity of the receptor, yeast growth assays were performed in the absence of an agonist. Results are shown in Figure 1B and 1C. In response to increasing concentrations of 3-AT yeast cell growth was dose-dependently decreased for yeast cells both in the presence and absence of wild-type hA$_1$AR (Figure 1B). The presence of hA$_1$AR resulted in a lower apparent potency of 3-AT. At a concentration of 4 mM 3-AT, the two curves showed the largest difference in growth as yeast cells with hA$_1$AR were still able to grow, while yeast cells transformed with empty vector hardly grew. Importantly, in this system mutant receptors with increased constitutive activity, i.e. CAMs, would show a larger response than wild-type hA$_1$AR, while mutant receptor with decreased constitutive activity, i.e. CIMs, would show a response in between wild-type hA$_1$AR and empty vector at this concentration of 3-AT (Figure 1B).

Cancer-related mutations had various effects on the constitutive activities of the hA$_1$AR (Figure 1C). All 5 mutants within the EL showed decreased constitutive activity compared to the wild-type hA$_1$AR. Interestingly, the 4 mutations located at the IL of the receptor showed a large variance in their constitutive activities. Specifically, mutant receptor L113F$^{34.51}$, located at IL2, showed a significantly decreased constitutive activity. In contrast, increased constitutive activity was observed for mutant receptor L211R$^{5.69}$ and V215L^{IL3}, where the increase on V215L^{IL3} was not significant. Mutant receptors D221N^{IL3} and R308H$^{8.63}$, located at IL3 and the C-terminus respectively, did not behave significantly different from wild-type hA$_1$AR. Two other mutations located at the C-terminus hA$_1$AR, H306N$^{8.61}$ and I315V$^{C\text{-}term}$, were constitutively inactive.

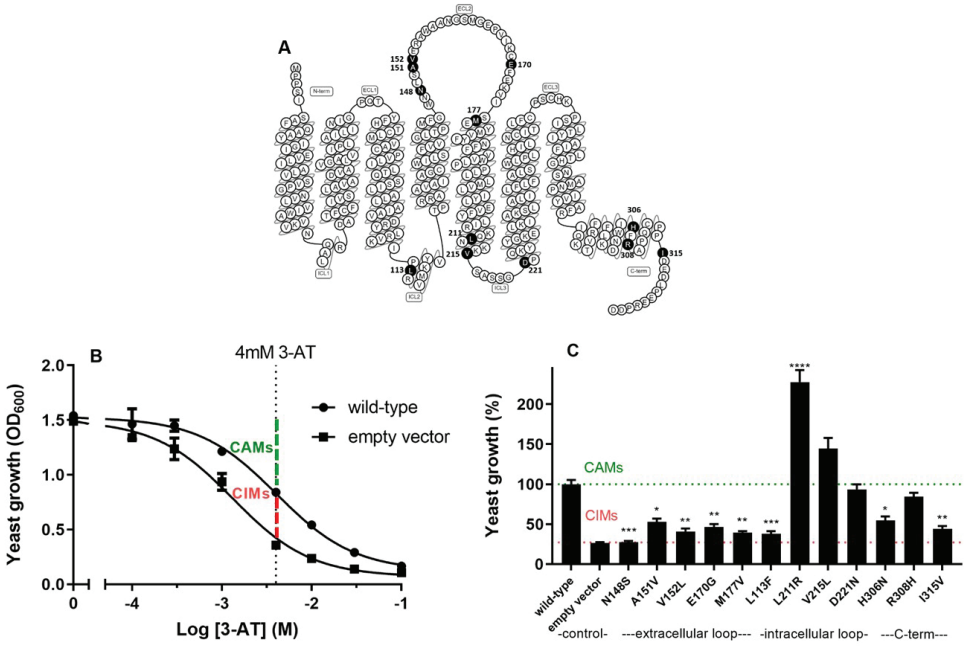

Figure 1. (A) Snake-plot of the wild-type hA_1AR. Mutated residues are marked in black. (B) Concentration-growth curves of yeast in the absence (empty vector) or presence of wild-type hA_1AR. A concentration of 4 mM 3-AT (dotted line), resulted in the largest assay window to detect either CAMs or CIMs. Specifically, mutant receptors with increased constitutive activity (CAMs) would show a higher growth level than wild-type hA_1AR (assay window depicted as green dotted line), while those with decreased constitutive activity (CIMs) would show a growth level lower than wild-type hA_1AR but higher than empty vector (assay window depicted as red dotted line). Combined graph is shown as mean ± SEM from three individual experiments performed in duplicate. (C) Constitutive activity of wild-type and 12 mutant hA_1ARs in presence of 4 mM 3-AT. Yeast growth in presence of wild-type hA_1AR was set to 100% (green dotted line) and the background of the selection medium was set to 0%. The yeast growth of empty vector is 26% (red dotted line). The bar graph is the combined result of three independent experiments performed in quadruplicate.
* $p < 0.05$; ** $p < 0.01$; *** $p < 0.001$; **** $p < 0.0001$ compared to wild-type hA_1AR, determined by using one-way ANOVA with Dunnett's post-test.

Characterization of receptor activation of mutant hA_1ARs

To further characterize the effects of cancer-related mutations on receptor activation concentration-growth curves were obtained for all 12 mutants hA_1ARs in response to the selective hA_1AR full agonist CPA (Figure 2 and Table 2). In this yeast system, wild-type hA_1AR showed a pEC_{50} value of 9.29 ± 0.07 and a maximum effect (E_{max}) of 5.37 ± 0.53 for CPA, and a constitutive activation level of 1.00 ± 0.04. Over half of the mutant receptors showed a decreased constitutive activity, but similar potency and efficacy values for CPA as at the wild-type hA_1AR (Figure 2 – dark blue curves and Table 2).

Within the mutant receptors of the EL, the largest change in receptor function was observed for mutant receptor E170G$^{45.51}$, which showed no response to CPA

(Figure 2A). Other mutations in the EL did not lead to such severe changes in the pharmacological behavior of the receptor, i.e. these mutant receptors could all be activated by CPA to reach a similar E_{max} as at wild-type hA_1AR with up to 10-fold decreased potency values. Among them, mutant receptors $N148S^{EL2}$, $V152L^{EL2}$ and $M177V^{5.37}$ showed significantly reduced pEC_{50} values of 8.54 ± 0.08, 8.80 ± 0.06 and 8.32 ± 0.06 (Table 2).

Mutant receptors located at the IL showed a more divergent behavior, unlike mutant receptors located at the EL (Figure 2B and Table 2). Mutant receptor $L113F^{34.51}$ showed a reduced basal activity and activation in response to CPA with both a decreased pEC_{50} value of 8.43 ± 0.13 and E_{max} value of 2.45 ± 0.30. Mutant receptors $V215L^{IL3}$ and $D221N^{IL3}$ did not show altered receptor function with similar dose – growth curves for CPA as on wild-type hA_1AR. The mutant receptor with increased constitutive activity, $L211R^{5.69}$ showed a similar potency value of 9.48 ± 0.14 and similar efficacy value of 5.33 ± 0.66 compared to wild-type hA_1AR. Of note, its high constitutive activity could be reduced by the inverse agonist, DPCPX with a pIC_{50} of 8.80 ± 0.15 to a similar level as on the wild-type hA_1AR (Figure 3).

Mutations located at the C-terminus had the least effect on receptor activation of the hA_1AR (Figure 2C and Table 2). All three mutant receptors could be activated to similar E_{max} values with similar pEC_{50} values of CPA (9.47 ± 0.07 on $H306N^{8.61}$, 9.48 ± 0.06 on $R308H^{8.63}$ and 9.14 ± 0.14 on $I315V^{C\text{-}term}$) as wild-type hA_1AR. As found in the screening of constitutive activity (Figure 1C), $H306N^{8.61}$ and $I315V^{C\text{-}term}$ had lower basal activity levels than wild-type hA_1AR.

Taken together, based on the different pharmacological effects of these mutant receptors, we characterized mutant receptor $L211R^{5.69}$ as CAM, mutant receptor E170G as a loss of function mutant (LFM), mutant receptors $N148S^{EL2}$, $A151V^{EL2}$, $V152L^{EL2}$, $M177V^{5.37}$, $L113F^{34.51}$, $H306N^{8.61}$ and $I315V^{C\text{-}term}$ as CIMs and mutant receptors $V215L^{IL3}$, $D221N^{IL3}$ and $R308H^{8.63}$ as no effect mutants (NEMs).

Ligand binding on wild-type and mutated hA_1AR

To further investigate mutant receptor function in a mammalian system, the 9 mutant receptors located at the ELs and ILs were selected. Mutations at these domains were expected to regulate the receptor-ligand interaction or receptor-G protein interaction. Therefore, wild-type and mutant receptors were transiently transfected into CHO cells. Cell membranes were collected and used in radioligand displacement assays (Figure 4 and Table 3). Receptor expression levels were measured by Western blot analysis where a band of the hA_1AR appeared around 37 kDa, and a non-specific band was seen at 15 kDa. As shown in Figure 4A, decreased expression levels for mutant receptors $L113F^{34.51}$, $N148S^{EL2}$, $V152L^{EL2}$, $E170G^{45.51}$, $M177V^{5.37}$, $L211R^{5.69}$ and $V215L^{IL3}$ were observed compared to wild-type hA_1AR (Figure 4A), while only mutant receptor $N148S^{EL2}$ showed significancy.

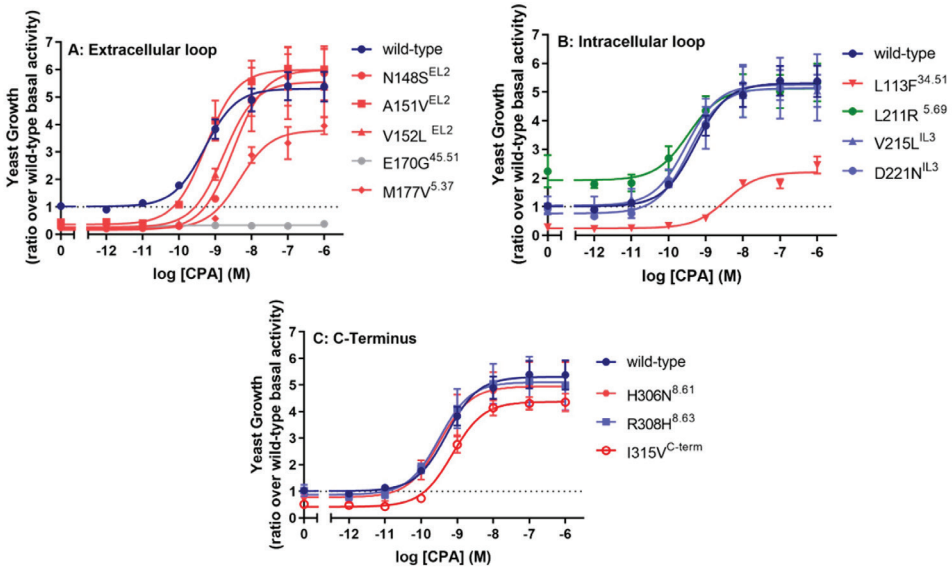

Figure 2. Concentration-response curves of the hA_1AR full agonist CPA at wild-type and mutated hA_1ARs. Data is separated for mutations located at (A) the extracellular loop, (B) the intracellular loop and (C) the C-terminus. Data were normalized as ratio over basal activity of wild-type hA_1AR (dotted line). Combined graphs are shown as mean ± SEM from at least three individual experiments performed in duplicate. CIMs are shown in red, CAMs in green, LFMs in grey and NEMs in blue.

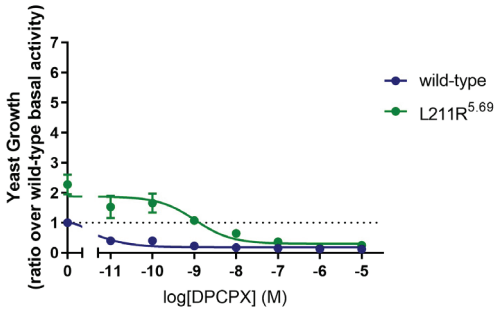

Figure 3. Concentration-inhibition curves of the hA_1AR inverse agonist DPCPX at the wild-type A_1AR and the CAM, $L211R^{5.69}$ Data were normalized as ratio over basal activity of wild-type hA_1AR (dotted line). Combined graphs are shown as mean ± SEM from at least three individual experiments performed in duplicate.

Homologous displacement experiments with [^{3}H]DPCPX and DPCPX resulted in a pK_D value of 8.42 ± 0.01 for the wild-type hA_1AR, which was not different from the values for mutant receptors $L113F^{34.51}$ and $L211R^{5.69}$ (8.48 ± 0.02 and 8.52 ± 0.05, Table 3). Mutant receptors $N148S^{EL2}$, $A151V^{EL2}$, $V152L^{EL2}$ and $D221N^{IL3}$ had decreased pK_D values of 8.15 ± 0.04, 8.22 ± 0.06, 8.19 ± 0.05 and 8.12 ± 0.05 (Table 3). Increased pK_D values were obtained on mutant receptors $E170G^{45.51}$ and $V215L^{IL3}$ (8.81 ± 0.04 and 8.65 ± 0.04, Table 3). All mutant receptors showed lower B_{max} values than the wild-type hA_1AR (2.92 ± 0.17 pmol/mg, Table 3), where mutant $V152L^{EL2}$ had the lowest expression level of 0.72 ± 0.05 pmol/mg. Notably, no specific binding

Table 2. *In vitro* pharmacological characterization of A_1AR mutants identified from cancer patient samples in yeast liquid growth assays, yielding information on level of constitutive activity, agonist potency and efficacy at these receptors.

Mutation	Basal†	pEC_{50}	E_{max}†	Type‡
Wild-type	1.00 ± 0.04	9.29 ± 0.07	5.37 ± 0.53	-
N148S^{EL2}	0.25 ± 0.0^{5***}	8.54 ± 0.08**	5.87 ± 0.98	CIM
A151V ^{EL2}	0.43 ± 0.02****	9.26 ± 0.13	6.00 ± 0.74	CIM
V152L ^{EL2}	0.33 ± 0.04***	8.80 ± 0.06*	5.52 ± 1.24	CIM
E170G$^{45.51}$	0.26 ± 0.04***	ND	ND	LFM
M177V$^{5.37}$	0.26 ± 0.02**	8.32 ± 0.06**	3.95 ± 0.31	CIM
L113F$^{34.51}$	0.28 ± 0.05**	8.43 ± 0.1^{3**}	2.45 ± 0.30***	CIM
L211R$^{5.69}$	2.24 ± 0.56*	9.48 ± 0.14	5.33 ± 0.66	CAM
V215L^{IL3}	1.07 ± 0.29	9.58 ± 0.08	5.04 ± 0.56	NEM
D221N^{IL3}	0.92 ± 0.19	9.48 ± 0.25	5.16 ± 1.16	NEM
H306N$^{8.61}$	0.80 ± 0.12	9.47 ± 0.07	4.94 ± 0.93	CIM
R308H$^{8.63}$	1.03 ± 0.22	9.48 ± 0.06	4.99 ± 0.93	NEM
I315V$^{C\text{-}term}$	0.52 ± 0.09*	9.14 ± 0.14	4.35 ± 0.33	CIM

Mutations are shown in the numbering of the hA_1AR amino acid sequence as well as according to the Ballesteros-Weinstein GPCR numbering system. Potency (pEC_{50}) and efficacy (E_{max}) values are shown as mean ± SEM obtained from at least three individual experiments performed in duplicate.
† values were calculated as ratio over basal activity of wild-type hA_1AR.
‡ types of mutants were depending on both screening of constitutive activity and receptor activation.
* $p < 0.05$; ** $p < 0.01$; *** $p < 0.001$ compared to wild-type hA_1AR, determined by a two-tailed unpaired Student's t-test.
ND: not detectable, CAM: constitutively active mutant, CIM: constitutively inactive mutant, LFM: loss of function mutant, NEM: no effect mutant

could be detected for mutant receptor M177V$^{5.37}$ in the presence of 1.6 nM [^{3}H] DPCPX (data not shown).

Next, heterologous displacement experiments were performed on wild-type and mutant hA_1ARs with the agonist CPA. Interestingly, for the wild-type hA_1AR the data was best fitted by a two-site model whereas the data was preferable fitted by a one-site model when DPCPX was used as a displacer (Figure 4B and 4C). With regard to CPA binding to mutant hA_1ARs, the two-site model was also preferred for mutant receptors L113F$^{34.51}$, N148S^{EL2}, V152L^{EL2}, E170G$^{45.51}$ and L211R$^{5.69}$. Conversely, for mutant receptors A151V^{EL2}, V215L^{IL3} and D221N^{IL3} a one-site binding model was preferred (Figure 4D and 4E). After fitting wild-type hA_1AR data to the two-site binding model, pK_i values of 8.89 ± 0.19 at the high affinity state and 6.65 ± 0.03 at the low affinity state were obtained with a fraction of 0.23 ± 0.02 for the high affinity state (Table 3). An altered pK_i value at the high affinity state was only obtained on mutant receptor V152L^{EL2} (7.49 ± 0.31) compared to wild-type hA_1AR. Interestingly, more diverse effects of mutant receptors on CPA binding were observed at the low affinity state. Mutant receptor L211R$^{5.69}$ showed an increased pK_i(low) value of 7.11 ± 0.06 compared to wild-type hA_1AR, while mutant receptors N148S^{EL2} and V152L^{EL2} had reduced values of 6.10 ± 0.09 and 6.02 ± 0.10 (Figure 4D, 4E and Table 3).

Table 3. B_{max} and pK_D values of [^{3}H]DPCPX and binding affinity of CPA on wild-type and mutant hA_1ARs.

	[^{3}H]DPCPX		CPA			
	B_{max} (pmol/mg) †	pK_D †	pK_i (high) ‡	pK_i (low) ‡	Fraction (high) ‡	pK_i §
Wild-type	2.92 ± 0.17	8.42 ± 0.01	8.89 ± 0.19	6.65 ± 0.03	0.23 ± 0.02	n.a.
L113F$^{34.51}$	1.22 ± 0.08****	8.48 ± 0.02	9.08 ± 0.20	6.81 ± 0.02	0.26 ± 0.02	n.a.
N148S^{EL2}	0.75 ± 0.07****	8.15 ± 0.04**	8.02 ± 0.10	6.10 ± 0.0^{9*}	0.22 ± 0.02	n.a.
A151V^{EL2}	0.89 ± 0.22****	8.22 ± 0.06*	n.a.	n.a.	n.a.	6.40 ± 0.05**
V152L^{EL2}	0.72 ± 0.08****	8.19 ± 0.05**	7.49 ± 0.31**	6.02 ± 0.10**	0.40 ± 0.08	n.a.
E170G$^{45.51}$	1.52 ± 0.04****	8.81 ± 0.04****	8.33 ± 0.36	6.77 ± 0.14	0.39 ± 0.09	n.a.
M177V$^{5.37}$	ND	ND	ND	ND	ND	ND
L211R$^{5.69}$	1.20 ± 0.10****	8.52 ± 0.03	8.35 ± 0.16	7.11 ± 0.06*	0.20 ± 0.07	n.a.
V215L^{IL3}	1.00 ± 0.06****	8.65 ± 0.04**	n.a.	n.a.	n.a.	6.87 ± 0.08
D221N^{IL3}	1.56 ± 0.11****	8.12 ± 0.05***	n.a.	n.a.	n.a.	6.40 ± 0.06**

B_{max}, pK_D, pK_i and fraction values are shown as mean ± SEM obtained from three individual experiments performed in duplicate.
* $p < 0.05$; ** $p < 0.01$; *** $p < 0.001$; **** $p < 0.0001$ compared to wild-type hA_1AR, as determined by one-way ANOVA with Dunnett's post-test.
† Values obtained from homologous displacement of ~1.6, 4.5 and 10 nM [^{3}H]DPCPX from transiently transfected wild-type and mutant CHO-hA_1AR membranes at 25°C.
‡ In cases where the CPA displacement curve fitted best to a two-site model pK_i (high), pK_i (low) and Fraction (high) values were determined by fitting data to a two-site model.
§ In cases where the CPA displacement curve fitted best to a one-site model pK_i values are provided. For comparison, the pK_i value of wild-type hA_1AR (6.85 ± 0.06) was used determined by fitting data to a one-site model.
ND: not detectable
n.a.: not applicable, as this was not statistically preferred

To be able to compare to some "one-site" mutants, a pKi value of 6.85 ± 0.06 was determined for wild-type hA_1AR by fitting the data to the one-site model (Table 3). Compared to wild-type hA_1AR, mutant receptors A151V^{EL2} and D221N^{IL3} showed decreased affinity values (pK_i) of 6.40 ± 0.05 and 6.40 ± 0.06 for CPA.

[^{35}S]GTPγS functional assay

CHO cell membranes transiently transfected with wild-type hA_1AR and 9 mutant receptors were further evaluated in a [^{35}S]GTPγS-binding assay. In this system, the wild-type A_1AR had a potency value of 8.80 ± 0.09 for CPA and an E_{max} value of 1.67 ± 0.07. In the mammalian system, all mutant receptors could be activated by CPA with some differences in efficacy or potency values compared to wild-type hA_1AR, similar to the yeast system with one exception being mutant receptor E170G$^{45.51}$. This receptor was characterized as a LFM in the yeast system, while in the [^{35}S]GTPγS-binding assay it behaved similar to wild-type hA_1AR (Figure 5A, 5B and Table 4). Mutant receptors N148S^{EL2}, V152L^{EL2} and M177V$^{5.37}$ showed a reduced potency for CPA in the yeast system, and also showed decreased potency values in the [^{35}S]GTPγS-binding assay, although this decrease was not significant for V152L^{EL2}

(Figure 5A and Table 4). Mutant receptor M177V$^{5.37}$ behaved similarly in the yeast and mammalian assay, i.e. the potency of CPA decreased more than one log-unit and the efficacy remained unchanged (Figure 5A).

While data on mutant receptors in EL were very similar in the yeast and mammalian system, mutant receptors in IL showed more divergence in receptor pharmacology between systems (Figure 5B and Table 4). Mutant receptor L113F$^{34.51}$, was characterized as a CIM with decreased potency and efficacy in the yeast system, while it did not behave differently from the wild-type hA$_1$AR in the [^{35}S]GTPγS-binding assay (Figure 5B and Table 4). Mutant receptor L211R$^{5.69}$, characterized as a CAM in

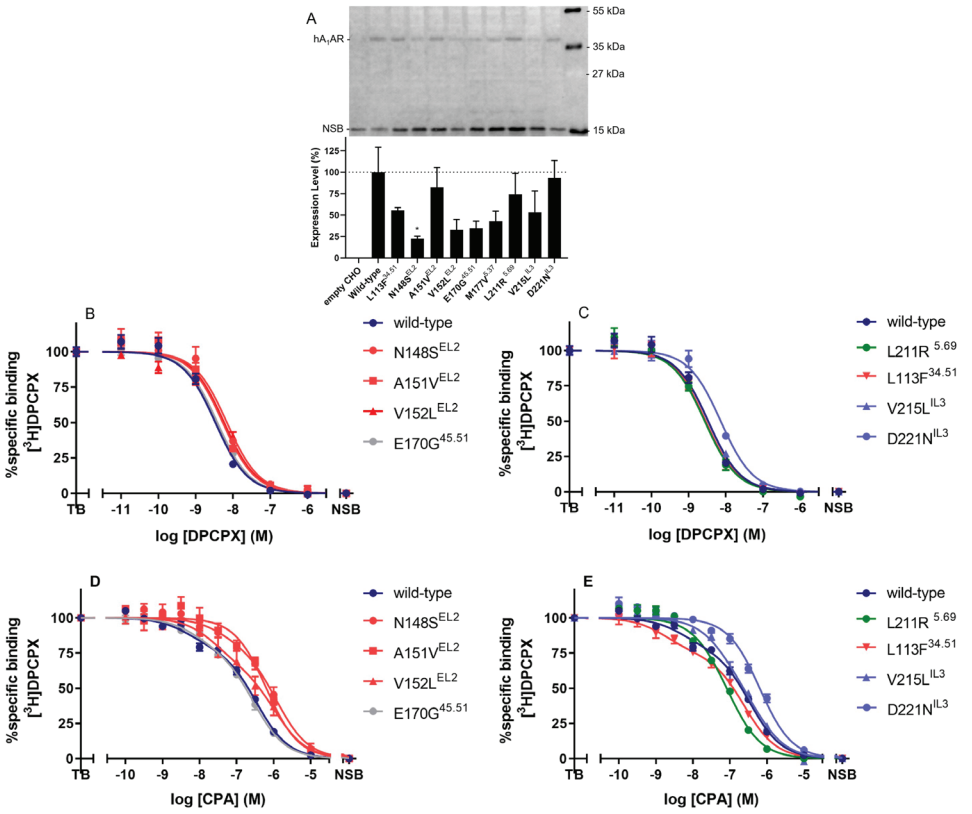

Figure 4. (A) Western blot analysis of CHO cell membranes transiently transfected with wild-type and mutant hA$_1$ARs. The specific hA$_1$AR band was found around 37 kDa, whereas a non-specific band (NSB) was found around 15 kDa. Expression level of wild-type hA$_1$AR relative to NSB was set to 100%, while expression level of mock transfected CHO cell membrane (empty CHO) relative to NSB was set to 0%. * $p < 0.05$ compared to wild-type hA$_1$AR, determined by using one-way ANOVA with Dunnett's post-test. (B-E) Displacement of specific [^{3}H]DPCPX binding to the transiently transfected wild-type hA$_1$AR, as well as 9 mutant receptors located at the extracellular loops (EL) (B and D) and intracellular loops (IL) (C and E), on CHO cell membranes by DPCPX and CPA. Combined graphs are shown as mean ± SEM from three individual experiments, each performed in duplicate. CIMs are shown in red, CAMs in green, LFMs in grey and NEMs in blue.

the yeast system, did not show altered constitutive activity in the mammalian system. Lastly, V215L^{IL3} and D221N^{IL3} were characterized as NEMs in the yeast system, but showed distinct pharmacological behavior in mammalian cells. Specifically, compared to the wild-type hA$_1$AR, both mutant receptors showed similar constitutive activity and potency values, but significantly decreased efficacy values (1.38 ± 0.04 on V215L^{IL3} and 1.35 ± 0.04 D221N^{IL3}) in response to CPA in the [^{35}S]GTPγS-binding assay (Figure 5B and Table 4).

For wild-type and all mutant hA$_1$AR receptors, the CPA-mediated activation was inhibited by the inverse agonist DPCPX (Figure 5C, 5D and Table 4). The activation level of mutant receptors L113F$^{34.51}$, N148S^{EL2}, V152L^{EL2} and L211R$^{5.69}$ was decreased to wild-type hA$_1$AR level with similar pIC$_{50}$ values for DPCPX as for the wild-type hA$_1$AR (8.00 ± 0.11 for wild-type, 7.88 ± 0.06 for L113F$^{34.51}$, 7.64 ± 0.05 for N148S^{EL2}, 7.58 ± 0.07 for V152L^{EL2} and 7.82 ± 0.26 for L211R$^{5.69}$). Decreased potency values of 7.50 ± 0.16 and 7.54 ± 0.05 for DPCPX were observed on mutant receptor A151V^{EL2} and D221N^{IL3} respectively, while the activation levels of these two mutant receptors could be reduced to wild-type hA$_1$AR level. For mutant receptors E170G$^{45.51}$ and V215L^{IL3}, the agonist-mediated receptor activation levels were decreased to a significantly lower level than wild-type hA$_1$AR (0.92 ± 0.01 for wild-type hA$_1$AR, 0.78

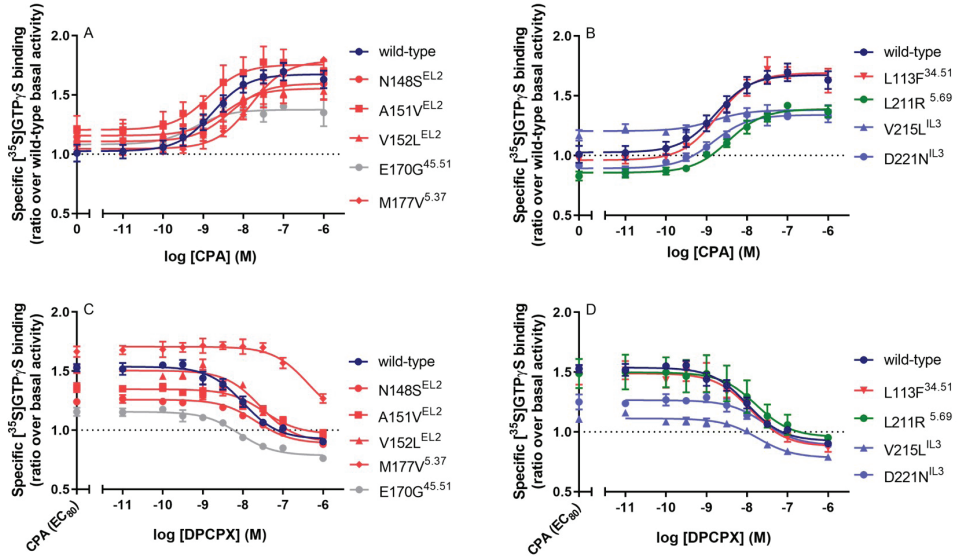

Figure 5. CPA-stimulated [^{35}S]GTPγS binding to transiently transfected wild-type hA$_1$AR and 9 mutant receptors located at the extracellular loops (EL) (A and C) and intracellular loops (IL) (B and D) on CHO cell membranes. (A and B) Receptor activation of wild-type and mutant receptors in response to CPA. Data were normalized as ratio over basal activity of wild-type hA$_1$AR. (C and D) Concentration-inhibition curves of DPCPX with the presence of CPA at the concentration of EC$_{80}$ for wild-type and mutant hA$_1$AR. Data were normalized as ratio over basal activity of wild-type or mutant hA$_1$AR. Combined graphs were shown as mean ± SEM obtained from three different experiments each performed in duplicate. CIMs are shown in red, CAMs in green, LFMs in grey and NEMs in blue.

± 0.01 for E170G$^{45.51}$ and 0.78 ± 0.02 for V215L^{IL3}), though the potency values of DPCPX remained unchanged. Of note, the inhibitory potency of DPCPX on mutant receptor M177V$^{5.37}$ was decreased the most with a pIC_{50} of 6.31 ± 0.08, where basal wild-type hA_1AR activation levels could still not be reached in presence of 1 μM DPCPX (Figure 5C and Table 4). This significantly lower potency value of DPCPX on the mutant receptor M177V$^{5.37}$ is in line with the observation that no binding of [^{3}H] DPCPX was detected at this mutant receptor (data not shown).

Table 4. Potency and efficacy of CPA and DPCPX in [^{35}S]GTPγS binding assays on wild-type and mutant hA_1ARs.

	CPA			DPCPX	
	Basal†	**pEC_{50}**	**E_{max} †**	**pIC_{50}**	**I_{max} ‡**
Wild-type	1.00 ± 0.06	8.80 ± 0.09	1.67 ± 0.07	8.00 ± 0.11	0.92 ± 0.01
L113F$^{34.51}$	0.96 ± 0.02	8.75 ± 0.07	1.69 ± 0.09	7.88 ± 0.06	0.88 ± 0.03
N148S^{EL2}	1.12 ± 0.09	8.29 ± 0.11*	1.60 ± 0.12	7.64 ± 0.05	0.89 ± 0.01
A151V^{EL2}	1.20 ± 0.10	8.88 ± 0.13	1.76 ± 0.12	7.50 ± 0.16*	0.97 ± 0.04
V152L^{EL2}	1.14 ± 0.05	8.49 ± 0.07	1.55 ± 0.08	7.58 ± 0.07	0.90 ± 0.01
E170G$^{45.51}$	1.09 ± 0.08	9.17 ± 0.11	1.38 ± 0.07	8.08 ± 0.10	0.78 ± 0.01**
M177V$^{5.37}$	1.04 ± 0.03	7.81 ± 0.06****	1.79 ± 0.02	6.31 ± 0.08****	1.27 ± 0.04****
L211R$^{5.69}$	0.85 ± 0.02	8.48 ± 0.09	1.39 ± 0.04	7.82 ± 0.15	0.95 ± 0.03
V215L^{IL3}	1.19 ± 0.04	8.93 ± 0.07	1.38 ± 0.04*	7.76 ± 0.14	0.78 ± 0.02**
D221N^{IL3}	0.90 ± 0.03	8.79 ± 0.21	1.35 ± 0.04*	7.54 ± 0.05*	0.88 ± 0.02

Basal, potency (pEC_{50} or pIC_{50}) and efficacy (E_{max} or I_{max}) values are shown as mean ± SEM obtained from at least three individual experiments performed in duplicate.
† values were calculated as ratio over basal activity of wild-type hA_1AR.
‡ values were calculated as ratio over basal activity of wild-type or mutant hA_1AR.
* $p < 0.05$; ** $p < 0.01$; *** $p < 0.001$; **** $p < 0.0001$ compared to wild-type hA_1AR, as determined by one-way ANOVA with Dunnett's post-test.

Structural mapping and bioinformatics analysis of mutations

The mutations investigated in this study were mapped on the inactive A_1AR structure (5UEN) to provide structural hypotheses for the observed pharmacological effect (i.e. NEM, LFM, CAM and CIM) of the different mutations. Two residues in the intracellular region (V215L^{IL3} (NEM) and I315V$^{C\text{-}term}$ (CIM)) were not mapped, because this part of the receptor is unresolved in both active and inactive structures.

Mutations in the ELs are located close to one another, both sequentially and structurally (Figure 6A). Most mutations in the EL region cause relatively mild structural changes, as mutants residues mostly retain the properties of the wild-type hA_1AR residues, except the LFM E170G$^{45.51}$ (Figure 6B). This mutation dramatically interrupted receptor activation and is located next to the conserved residue C169$^{45.50}$ and F171$^{45.52}$, of which the latter is part of the orthosteric binding site. The M177V$^{5.35}$ mutation had a large effect on receptor-ligand recognition (both agonist and antagonist) and this mutation is found in direct contact with the cyclopentyl moieties

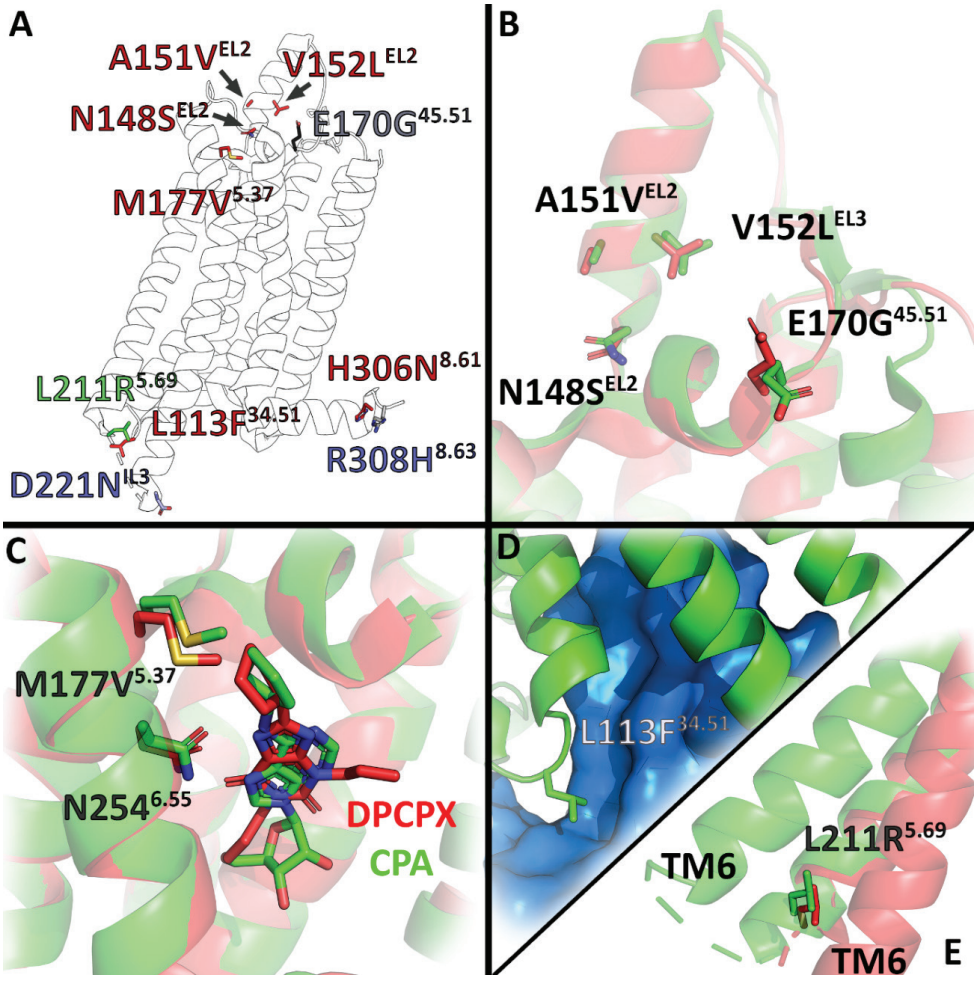

Figure 6. (A) Mutations from this study are mapped on the inactive A_1AR structure (5UEN). CIMs are shown in red, CAMs in green, LFMs in grey and NEMs in blue. (B-E) A close up is shown for the residues that showed the largest impact on receptor function upon mutation. The active structure (6D9H) is shown in green and the inactive in red (5UEN). Unresolved parts of the structure are shown as dashed cartoon representation. (B) Close up of the N148^{EL2}, A151^{EL2}, V152^{EL2}, E170$^{45.51}$ mutations located in the ELs. (C) Close up of the M177V$^{5.35}$ mutation in the orthosteric binding site. The reference ligands CPA (green) and DPCPX (red) used in this study are shown as sticks. (D) Close up of the L113F$^{34.51}$ mutation, which is found in the A_1AR-G protein interface. The G protein is shown in blue with surface representation. (E) Close-up of the L211R$^{5.69}$ mutation located at the bottom of TM5.

of both reference ligands used in this study (Figure 6C).

For the IL mutations, most constitute small changes in structural properties, with an exception for the two mutations L113F$^{34.51}$ (Figure 6D) and L211R$^{5.69}$ (Figure 6E), which are positioned close to the A_1AR – G protein interface. Moreover, L211$^{5.69}$ is situated in TM6, which undergoes a large conformational change upon receptor

activation. Notably, mutations on these residues exerted a large effect on receptor activation in yeast cells, but were found not to significantly alter receptor function in mammalian cells (compare Table 2 and 4).

Discussion

GPCR mutations are known to make alterations to receptor pharmacology by altering cell surface expression, GPCR-ligand interaction, basal activity and / or GPCR-G protein interaction, which can result in various disease phenotypes [38]. Additionally, it has been shown that various GPCR mutations are involved in cancer progression in different types of cancer [10,39], yet the role of these mutations in cancer is not fully characterized. Previous structural studies on hA_1AR indicated that some residues are crucial to ligand binding and receptor activation [21,35,36,40]. Moreover, crystal structures of hA_1AR have been published, which provided us with more structural information in the inactive receptor state [35,41] and in G protein-coupling [36]. Therefore, in this study we investigated 12 single-site point mutations located at the ELs, ILs and C-term of A_1AR that were obtained from The Cancer Genome Atlas (TCGA) [20]. These mutations were subsequently examined in the *S. cerevisiae* system and mammalian system to enrich our insight of the receptor activation mechanism in respect of cancer progression.

Mutations in the extracellular loops

All of the mutant receptors in the extracellular loops were located at EL2. EL2 of wild-type hA_1AR is known to be a positive regulator of receptor activation, as alanine mutations in this loop have been found to have negative regulatory effects[21]. Similarly, most of the EL2 mutant receptors in this study (i.e. $N148S^{EL2}$, $A151V^{EL2}$, $V152L^{EL2}$ and $M177V^{5.37}$) led to a decrease in constitutive activity (Figure 1B), while the maximal activation levels were not influenced in response to CPA (Figure 2A and Table 2). According to the two-state-receptor model[42], in CIMs the equilibrium is shifted from the active (R*) to the inactive (R) receptor conformation. Supporting, these mutant receptors $N148S^{EL2}$ and $V152L^{EL2}$ showed lower potency and affinity of CPA compared to the wild-type hA_1AR. Moreover, mutant receptor $A151V^{EL2}$ preferred a one-site CPA binding model, which showed that the equilibrium was shifted to one certain receptor conformation[43]. Interestingly, mutant receptors $N148S^{EL2}$, $A151V^{EL2}$, $V152L^{EL}$ showed a significantly lower affinity of DPCPX. It has been reported that these residues modulate ligand residence time of both agonist and antagonist of A_1AR[44]. Therefore, it is possible that these mutations indirectly affect CPA's and DPCPX's dissociation kinetics from the hA_1AR binding pocket. Notably, decreased potency of CPA was observed on mutant receptor $M177V^{5.35}$ in both the yeast and mammalian system (Figure 2A, 5A and Table 2, 4). Mutant receptor $M177V^{5.35}$ also showed a decreased potency for DPCPX (Figure 5C), which was corroborated by the loss of a [^{3}H]DPCPX window in the displacement experiments (Table 4). A similar

result has been reported by Nguyen *et al*. that introduced an alanine mutation at residue M177$^{5.35}$, resulting in a decreased affinity of DPCPX and full agonist NECA, indicating this residue is essential for ligand recognition[40]. Specifically, residue M177$^{5.35}$, together with residues L253$^{6.54}$ and T257$^{6.57}$, has been shown to form a hydrophobic pocket that engages the xanthine moiety of DPCPX[35]. Of note, the methionine at residue 5.35 is conserved among all adenosine receptors[45], which also indicates its essential role in the orthosteric binding site.

A complete loss of activation was observed for mutant receptor E170G$^{45.51}$ in the yeast system. However, it could be activated by CPA to a lower level with similar potency at the wild-type hA_1AR in the mammalian system. This CPA-mediated receptor activation could be reduced by DPCPX to a significantly lower level than wild-type hA_1AR (Figure 5C), indicating that mutant receptor E170G$^{45.51}$ might be constitutively active in the mammalian system. Residue E170$^{45.51}$ is situated between residues F171$^{45.52}$ and C169^{EL2}, where F171$^{45.52}$ is in the orthosteric binding pocket and residue C169^{EL2} forms the highly conserved Class A GPCR disulfide bond with C80$^{3.25}$[35,36]. Due to the lack of a side chain in glycine, replacing glutamic acid with glycine at residue 170 makes it prone to flexibility, which often leads to disruptions in protein structure[46]. The introduced flexibility might open up space around F171$^{45.52}$ and possibly even lead to W247$^{6.48}$ ('toggle switch') bending away from the binding pocket, resulting in disruption of the 'ligand-binding cradle'[47]. In turn, this might lead to an incomplete functionality of the receptor.

Mutations in the intracellular loops

Compared to mutant receptors from other locations in hA_1AR, mutant receptors in intracellular loops showed diverse effects on receptor pharmacology. Mutant receptors V215L^{IL3} and D221N^{IL3} were characterized as NEMs in the yeast system, while mutant receptor L211R$^{5.69}$ and L113F$^{34.51}$ behaved as CAM and CIM, respectively (Table 2). However, these mutational effects on receptor activation were not as clearly observed in the mammalian system.

The CIM L113F$^{34.51}$, located in the middle of IL2, showed not only low constitutive activity, but also a prominently decreased potency and efficacy of CPA in the yeast system (Figure 1B, 2B and Table 2). However, on the CHO cell membranes, the affinity, potency and efficacy of neither DPCPX or CPA were influenced by the phenylalanine mutation at residue L113$^{34.51}$. It has been shown that residue L113$^{34.51}$ in hA_1AR forms a Van der Waals interaction with the residue I344 (GH5.15) in $G\alpha_{i2}$[36]. This receptor-G protein interaction is also seen at other GPCRs, such as the muscarinic acetylcholine receptor M_1 (M_1R), where mutant receptor L131F$^{34.51}$ has also been shown not to influence G protein coupling[48]. Additionally, bulky hydrophobic amino acids at residue 34.51 commonly occur among GPCRs, indicating that the introduction of phenylalanine at residue L113$^{34.51}$ in hA_1AR should not significantly alter receptor - G protein coupling[45]. Therefore, the altered receptor pharmacology on mutant receptor L113F$^{34.51}$ in the yeast system might be specific for the receptor-

yeast G protein interaction.

CAM L211R$^{5.69}$, located at the end of TM5 and the beginning of IL3, showed a high activation level in the absence of an agonist in the yeast strain MMY24, but not in the mammalian system. The increased constitutive activity was reduced to wild-type hA_1AR level by the inverse agonist DPCPX (Figure 3), indicating that hA_1AR is not locked in an active conformation by mutation L211R$^{5.69}$. Based on the two-state receptor model[42], elevated constitutive activity is a result of the mutant receptor being more in the active state than the wild-type hA_1AR[49]. While the increased constitutive activity was not observed on CHO cell membranes transiently transfected by mutant receptor L211R$^{5.69}$, the affinity of CPA was increased on the mutant receptor L211R$^{5.69}$ (Figure 4C and Table 3). This indicated that the receptor might be in a more activated state that agonists prefer to bind to. Although L5.69 is completely conserved among all adenosine receptors, structural studies on residue 5.69 are limited, due to the high flexibility and minor effects in receptor function of IL3[50]. It has been shown that L211$^{5.69}$ interacts with K346 (GH5.19) and F355 (GH5.26) in Gα_{i2} by Van der Waals interactions[36,51]. Therefore, the divergent mutational effects observed between the yeast and mammalian system are likely due to the positions of these mutations close to the A_1AR – G protein interface, which is arguably different between mammalian and yeast cells even though the yeast system uses a partially humanized G protein[52].

Mutations in the C-terminus

In the C-terminus, CIMs H306N$^{8.61}$ and I315V$^{C\text{-term}}$ showed decreased constitutive activity, while the potency and efficacy of an agonist remained the same as for the wild-type hA_1AR. Moreover, mutant receptor R308H$^{8.63}$ was characterized as NEM (Figure 2C and Table 2). From a crystal structure of hA_1AR-G_i complex, it has been concluded that the C-terminus of the Gα_i subunit mainly interacts with the cytoplasmic end of TM2, TM3, TM5, TM6 and TM7, as well as the beginning of helix 8[36]. However, since mutant receptors H306N$^{8.61}$, R308H$^{8.63}$ and I315V$^{C\text{-term}}$ are located at the end part of helix 8, the receptor-G protein interaction is probably not affected much. Hence, the constitutive activity and receptor activation were not dramatically altered by these cancer-related mutations.

Potential role for hA_1AR mutations in cancer

ARs have been found to be involved in cancer biology[9,10]. In particular, multiple antagonistic antibodies and small molecule inhibitors against adenosine A_{2A} and A_{2B} receptors have been developed and display therapeutic efficacy in clinical trials against different solid tumors[10]. Anti-proliferative effects of hA_1AR activation have been identified in colon cancer, breast cancer, glioblastoma and leukemia[11,18,53]. The LFM E170G$^{45.51}$, identified from colon cancer, might therefore play a pro-proliferative role in cancer development. Interestingly in melanoma cells, deletion or blockade of hA_1AR suppressed cell proliferation but induced PD-L1 upregulation, resulting in compromised anti-tumor immunity[54]. Moreover, preclinical observations showed

that hA_1AR blockade by DPCPX inhibits cancer cell proliferation and promotes cell apoptosis[15,55,56]. Mutant receptors with altered receptor-ligand interaction, for example $N148S^{EL2}$, $V152L^{EL2}$ and $M177V^{5.35}$ in this study, may thus result in mis-dosing while using these small molecules as therapeutic approaches. Studies on GPCR heteromers provided evidence for the presence of hA_1AR[57]. A mutation with a mild impact on hA_1AR functionality was shown to play a pathogenic role in Parkinson's disease via a heteromeric complex with the dopamine D_1 receptor[58]. Analogously, mutant hA_1ARs may alter cancer biology through heteromers or oligomers, but further studies are warranted focusing on the role of hA_1AR heteromers in cancer progression. Although some of the cancer-related mutations in hA_1AR have a dramatic impact on receptor functionality, these effects are unlikely to be cancer-driving due to their lower frequency in cancer patients compared to known driver mutations e.g., RET proto-oncogene mutant M918T of which occurs in 50% of sporadic medullary thyroid carcinoma[20,59].

In conclusion, 12 cancer-related somatic mutations located at the extracellular, intracellular loops and C-terminus of the adenosine A_1 receptor were retrieved from TCGA and characterized in a robust yeast system, with follow-up in a mammalian system. The present study taught us that the yeast system is suitable for initial receptor pharmacology screening on mutations located outside the receptor-G protein interaction interface, and enabled us to identify mutations with dramatic effect on ligand binding and receptor activation. These mutations in the A_1AR may also regulate cell proliferation and migration in cancer cell lines, and thus might be further involved in cancer progression. Further studies are needed to investigate mutation-mediated receptor activation in a disease-relevant system. Together with the results from this study and the increasing evidence supporting the involvement of A_1AR in cancer[9,10,15,16,54], this will shed further light on the role of the A_1AR in cancer progression, which eventually may result in improved cancer therapy.

References

1. Fredriksson, R., Lagerström, M. C., Lundin, L.-G. & Schiöth, H. B. The G-protein-coupled receptors in the human genome form five main families. Phylogenetic analysis, paralogon groups, and fingerprints. *Mol. Pharmacol.* **63**, 1256–72 (2003).
2. Vassilatis, D. K. *et al.* The G protein-coupled receptor repertoires of human and mouse. *Proc. Natl. Acad. Sci.* **100**, 4903–4908 (2003).
3. Lagerström, M. C. & Schiöth, H. B. Structural diversity of G protein-coupled receptors and significance for drug discovery. *Nat. Rev. Drug Discov.* **7**, 339–57 (2008).
4. Pierce, K. L., Premont, R. T. & Lefkowitz, R. J. Seven-transmembrane receptors. *Nat. Rev. Mol. Cell Biol.* **3**, 639–650 (2002).
5. Kan, Z. *et al.* Diverse somatic mutation patterns and pathway alterations in human cancers. *Nature* **466**, 869–73 (2010).
6. Lappano, R. & Maggiolini, M. GPCRs and cancer. *Acta Pharmacol. Sin.* **33**, 351–362 (2012).
7. Dorsam, R. T. & Gutkind, J. S. G-protein-coupled receptors and cancer. *Nat. Rev. Cancer* **7**, 79–94 (2007).
8. Fredholm, B. B., IJzerman, A. P., Jacobson, K. a, Klotz, K. N. & Linden, J. International Union of Pharmacology. XXV. Nomenclature and classification of adenosine receptors. *Pharmacol. Rev.* **53**, 527–52 (2001).
9. Merighi, S. *et al.* A glance at adenosine receptors: novel target for antitumor therapy. *Pharmacol. Ther.* **100**, 31–48 (2003).
10. Sek, K. *et al.* Targeting Adenosine Receptor Signaling in Cancer Immunotherapy. *Int. J. Mol. Sci.* **19**, 3837 (2018).
11. Gessi, S., Merighi, S., Sacchetto, V., Simioni, C. & Borea, P. A. Adenosine receptors and cancer. *Biochim. Biophys. Acta* **1808**, 1400–1412 (2011).
12. Johnston, J. B. *et al.* Diminished adenosine A, receptor expression on macrophages in brain and blood of patients with multiple sclerosis. *Ann. Neurol.* **49**, 650–658 (2001).

13. Borea, P. A., Gessi, S., Merighi, S., Vincenzi, F. & Varani, K. Pharmacology of Adenosine Receptors: The State of the Art. *Physiol. Rev.* **98**, 1591–1625 (2018).
14. Merighi, S. *et al.* Pharmacological and biochemical characterization of adenosine receptors in the human malignant melanoma A375 cell line. *Br. J. Pharmacol.* **134**, 1215–1226 (2001).
15. Zhou, Y. *et al.* The Adenosine A_1 Receptor Antagonist DPCPX Inhibits Tumor Progression via the ERK/JNK Pathway in Renal Cell Carcinoma. *Cell. Physiol. Biochem.* **43**, 733–742 (2017).
16. Mirza, A. *et al.* RNA interference targeting of A_1 receptor-overexpressing breast carcinoma cells leads to diminished rates of cell proliferation and induction of apoptosis. *Cancer Biol. Ther.* **4**, 1355–1360 (2005).
17. Dastjerdi, M. N., Rarani, M. Z., Valiani, A. & Mahmoudieh, M. The effect of adenosine A_1 receptor agonist and antagonist on p53 and caspase 3, 8, and 9 expression and apoptosis rate in MCF-7 breast cancer cell line. *Res. Pharm. Sci.* **11**, 303–310 (2016).
18. Saito, M., Yaguchi, T., Yasuda, Y., Nakano, T. & Nishizaki, T. Adenosine suppresses CW2 human colonic cancer growth by inducing apoptosis via A_1 adenosine receptors. *Cancer Lett.* **290**, 211–215 (2010).
19. Synowitz, M. *et al.* A_1 Adenosine Receptors in Microglia Control Glioblastoma-Host Interaction. *Cancer Res.* **66**, 8550–8557 (2006).
20. *Broad Institute TCGA Genome Data Analysis Center (2016): Analysis-ready standardized TCGA data from Broad GDAC Firehose stddata_2015_08_21 run. Broad Institute of MIT and Harvard.* (2016). doi:10.7908/C18W3CNQ
21. Peeters, M. C. *et al.* The role of the second and third extracellular loops of the adenosine A_1 receptor in activation and allosteric modulation. *Biochem. Pharmacol.* **84**, 76–87 (2012).
22. Peeters, M. C., van Westen, G. J. P., Li, Q. & IJzerman, A. P. Importance of the extracellular loops in G protein-coupled receptors for ligand recognition and receptor activation. *Trends Pharmacol. Sci.* **32**, 35–42 (2011).
23. Peeters, M. C. *et al.* GPCR structure and activation: an essential role for the first extracellular loop in activating the adenosine A_{2B} receptor. *FASEB J.* **25**, 632–43 (2011).
24. Weinstein, J. N. *et al.* The Cancer Genome Atlas Pan-Cancer analysis project. *Nat. Genet.* **45**, 1113–1120 (2013).
25. UniProt: the universal protein knowledgebase. *Nucleic Acids Res.* **45**, D158–D169 (2017).
26. Ballesteros, J. A. & Weinstein, H. Integrated methods for the construction of three-dimensional models and computational probing of structure-function relations in G protein-coupled receptors. in *Methods in Neurosciences* **25**, 366–428 (1995).
27. Isberg, V. *et al.* Generic GPCR residue numbers – aligning topology maps while minding the gaps. *Trends Pharmacol. Sci.* **36**, 22–31 (2015).
28. Liu, R., Nahon, D., le Roy, B., Lenselink, E. B. & IJzerman, A. P. Scanning mutagenesis in a yeast system delineates the role of the NPxxY(x)5,6F motif and helix 8 of the adenosine A_{2B} receptor in G protein coupling. *Biochem. Pharmacol.* **95**, 290–300 (2015).
29. Yang, X. *et al.* Design and pharmacological profile of a novel covalent partial agonist for the adenosine A_1 receptor. *Biochem. Pharmacol.* **180**, 114144 (2020).
30. Dowell, S. J. & Brown, A. J. Yeast Assays for G Protein-Coupled Receptors. in *Methods in molecular biology (Clifton, N.J.)* (ed. Filizola, M.) **552**, 213–229 (Springer New York, 2009).
31. Longo, P. A., Kavran, J. M., Kim, M. S. & Leahy, D. J. Transient mammalian cell transfection with polyethylenimine (PEI). *Methods Enzymol.* **529**, 227–240 (2013).
32. Heitman, L. H. *et al.* A Series of 2,4-Disubstituted Quinolines as a New Class of Allosteric Enhancers of the Adenosine A_3 Receptor. *J. Med. Chem.* **52**, 926–931 (2009).
33. Smith, P. K. *et al.* Measurement of protein using bicinchoninic acid. *Anal. Biochem.* **150**, 76–85 (1985).
34. de Ligt, R. A. F., Rivkees, S. A., Lorenzen, A., Leurs, R. & IJzerman, A. P. A "locked-on," constitutively active mutant of the adenosine A_1 receptor. *Eur. J. Pharmacol.* **510**, 1–8 (2005).
35. Glukhova, A. *et al.* Structure of the Adenosine A_1 Receptor Reveals the Basis for Subtype Selectivity. *Cell* **168**, 867-877.e13 (2017).
36. Draper-Joyce, C. J. *et al.* Structure of the adenosine-bound human adenosine A_1 receptor–Gi complex. *Nature* **558**, 559–563 (2018).
37. Cheng, Y.-C. & Prusoff, W. H. Relationship between the inhibition constant (KI) and the concentration of inhibitor which causes 50 per cent inhibition (I50) of an enzymatic reaction. *Biochem. Pharmacol.* **22**, 3099–3108 (1973).
38. Stoy, H. & Gurevich, V. V. How genetic errors in GPCRs affect their function: Possible therapeutic strategies. *Genes Dis.* **2**, 108–132 (2015).
39. O'Hayre, M. *et al.* The emerging mutational landscape of G proteins and G-protein-coupled receptors in cancer. *Nat. Rev. Cancer* **13**, 412–24 (2013).
40. Nguyen, A. T. N. *et al.* Extracellular Loop 2 of the Adenosine A_1 Receptor Has a Key Role in Orthosteric Ligand Affinity and Agonist Efficacy. *Mol. Pharmacol.* **90**, 703–714 (2016).
41. Cheng, R. K. Y. *et al.* Structures of Human A_1 and A_{2A} Adenosine Receptors with Xanthines Reveal Determinants of Selectivity. *Structure* **25**, 1275-1285.e4 (2017).
42. Leff, P. The two-state model of receptor activation. *Trends Pharmacol. Sci.* **16**, 89–97 (1995).
43. Guo, D. *et al.* A two-state model for the kinetics of competitive radioligand binding. *Br. J. Pharmacol.* **175**, 1719–1730 (2018).
44. Nguyen, A. T. N. *et al.* Role of the Second Extracellular Loop of the Adenosine A_1 Receptor on Allosteric Modulator Binding, Signaling, and Cooperativity. *Mol. Pharmacol.* **90**, 715–725 (2016).
45. Isberg, V. *et al.* GPCRdb: an information system for G protein-coupled receptors. *Nucleic Acids Res.* **44**, D356–D364 (2016).
46. Yohannan, S., Faham, S., Yang, D., Whitelegge, J. P. & Bowie, J. U. The evolution of transmembrane helix kinks and the structural diversity of G protein-coupled receptors. *Proc. Natl. Acad. Sci.* **101**, 959–963 (2004).
47. Venkatakrishnan, A. J. *et al.* Molecular signatures of G-protein-coupled receptors. *Nature* **494**, 185–194 (2013).
48. Moro, O., Lameh, J., Högger, P. & Sadée, W. Hydrophobic amino acid in the i2 loop plays a key role in receptor-G protein coupling. *J. Biol. Chem.* **268**, 22273–6 (1993).
49. Kobilka, B. K. G protein coupled receptor structure and activation. *Biochim. Biophys. Acta - Biomembr.* **1768**, 794–807 (2007).
50. Dror, R. O. *et al.* Structural basis for nucleotide exchange in heterotrimeric G proteins. *Science*. **348**, 1361–1365 (2015).
51. Wang, J. & Miao, Y. Mechanistic Insights into Specific G Protein Interactions with Adenosine Receptors. *J. Phys. Chem. B* **123**, 6462–6473 (2019).
52. Brown, A. J. *et al.* Functional coupling of mammalian receptors to the yeast mating pathway using novel yeast/mammalian G protein α-subunit chimeras. *Yeast* **16**, 11–22 (2000).
53. Borea, P. A., Gessi, S., Merighi, S., Vincenzi, F. & Varani, K. Pathological overproduction: the bad side of adenosine. *Br. J. Pharmacol.* **174**, 1945–1960 (2017).
54. Liu, H. *et al.* ADORA1 Inhibition Promotes Tumor Immune Evasion by Regulating the ATF3-PD-L1 Axis. *Cancer Cell*

37, 324-339.e8 (2020).
55. Ma, H. *et al.* Dual Inhibition of Ornithine Decarboxylase and A_1 Adenosine Receptor Efficiently Suppresses Breast Tumor Cells. *Front. Oncol.* **11**, 1–10 (2021).
56. Zamani Rarani, M. *et al.* Adenosine A_1 Receptor Antagonist Up-regulates Casp3 and Stimulates Apoptosis Rate in Breast Cancer Cell Line T47D. *Int. Electron. J. Med.* **9**, 14–20 (2020).
57. Navarro, G. *et al.* Quaternary structure of a G-protein-coupled receptor heterotetramer in complex with Gi and Gs. *BMC Biol.* **14**, 1–12 (2016).
58. Nasrollahi-Shirazi, S. *et al.* Functional impact of the G279S substitution in the adenosine A_1-receptor (A_1R-G279S$^{7.44}$), a mutation associated with Parkinson's disease. *Mol. Pharmacol.* **98**, 250-266 (2020).
59. Gimm, O. *et al.* Over-representation of a germline RET sequence variant in patients with sporadic medullary thyroid carcinoma and somatic RET codon 918 mutation. *Oncogene* **18**, 1369–1373 (1999).